

Effect of plasmon-enhancement on photophysics in upconverting nanoparticles

Q.-C. Sun,¹ J. Casamada-Ribot,¹ V. Singh,¹ H. Mundoor,² I. I. Smalyukh,^{2,3,4}
and P. Nagpal^{1,3,4,*}

¹Department of Chemical and Biological Engineering, University of Colorado Boulder, Boulder, Colorado, USA

²Department of Physics, University of Colorado Boulder, Boulder, Colorado, USA

³Materials Science and Engineering, University of Colorado Boulder, Boulder, Colorado, USA

⁴Renewable and Sustainable Energy Institute (RASEI), University of Colorado Boulder, Boulder, Colorado, USA

*pnagpal@colorado.edu

Abstract: Surface plasmon polaritons (SPP) waves have been shown to significantly affect the near-field photophysical phenomenon. In particular, strong Coulombic interactions can enhance nearby non-linear optics and energy transfer process, while SPP waves also affect other photophysical processes like quenching observed in fluorescent and excitonic systems. Here, using different plasmonic substrates, we show the effect of plasmon-enhancement on quenching, phonon-assisted non-radiative decay, weak Purcell effect or electromagnetic field enhancement, and energy transfer rates of upconverting doped-lanthanide nanoparticles. While the resonant plasmons enhance the local electromagnetic field and the rate of energy transfer leading to enhanced upconversion photoluminescence of infrared radiation to visible light, it can also increase the quenching and non-radiative decay rates of photoexcited electron-hole pairs leading to losses and lower efficiency. These results can guide the design of optimized substrate geometry for using surface plasmons to modulate the photophysics in other applications too.

©2014 Optical Society of America

OCIS codes: (100.2960) Image analysis; (190.7220) Upconversion.

References and links

1. A. Shalav, B. S. Richards, T. Trupke, K. W. Kramer, and H. U. Gudel, "Application of NaYF₄: Er³⁺ up-converting phosphors for enhanced near-infrared silicon solar cell response," *Appl. Phys. Lett.* **86**(1), 013505 (2005).
2. B. M. van der Ende, L. Aarts, and A. Meijerink, "Lanthanide ions as spectral converters for solar cells," *Phys. Chem. Chem. Phys.* **11**(47), 11081–11095 (2009).
3. M. Nyk, R. Kumar, T. Y. Ohulchanskyy, E. J. Bergey, and P. N. Prasad, "High contrast in vitro and in vivo photoluminescence bioimaging using near infrared to near infrared up-conversion in Tm³⁺ and Yb³⁺ doped fluoride nanophosphors," *Nano Lett.* **8**(11), 3834–3838 (2008).
4. F. Wang and X. Liu, "Recent advances in the chemistry of lanthanide-doped upconversion nanocrystals," *Chem. Soc. Rev.* **38**(4), 976–989 (2009).
5. Y.-F. Wang, G.-Y. Liu, L.-D. Sun, J.-W. Xiao, J.-C. Zhou, and C.-H. Yan, "Nd³⁺-sensitized upconversion nanophosphors: efficient in vivo bioimaging probes with minimized heating effect," *ACS Nano* **7**(8), 7200–7206 (2013).
6. J. Zhao, D. Jin, E. P. Schartner, Y. Lu, Y. Liu, A. V. Zvyagin, L. Zhang, J. M. Dawes, P. Xi, J. A. Piper, E. M. Goldys, and T. M. Monro, "Single-nanocrystal sensitivity achieved by enhanced upconversion luminescence," *Nat. Nanotechnol.* **8**(10), 729–734 (2013).
7. F. Auzel, "Upconversion and anti-stokes processes with f and d ions in solids," *Chem. Rev.* **104**(1), 139–174 (2004).
8. M. Haase and H. Schäfer, "Upconverting nanoparticles," *Angew. Chem. Int. Ed. Engl.* **50**(26), 5808–5829 (2011).
9. F. Wang, Y. Han, C. S. Lim, Y. Lu, J. Wang, J. Xu, H. Chen, C. Zhang, M. Hong, and X. Liu, "Simultaneous phase and size control of upconversion nanocrystals through lanthanide doping," *Nature* **463**(7284), 1061–1065 (2010).

10. A. Polman and F. van Veggel, "Broadband sensitizers for erbium-doped planar optical amplifiers: review," *J. Opt. Soc. Am. B* **21**(5), 871–892 (2004).
11. S. Schietinger, T. Aichele, H.-Q. Wang, T. Nann, and O. Benson, "Plasmon-enhanced upconversion in single NaYF₄:Yb³⁺/Er³⁺ codoped nanocrystals," *Nano Lett.* **10**(1), 134–138 (2010).
12. F. Wang, R. Deng, J. Wang, Q. Wang, Y. Han, H. Zhu, X. Chen, and X. Liu, "Tuning upconversion through energy migration in core-shell nanoparticles," *Nat. Mater.* **10**(12), 968–973 (2011).
13. J. Wang, R. Deng, M. A. MacDonald, B. Chen, J. Yuan, F. Wang, D. Chi, T. S. A. Hor, P. Zhang, G. Liu, Y. Han, and X. Liu, "Enhancing multiphoton upconversion through energy clustering at sublattice level," *Nat. Mater.* **13**(2), 157–162 (2014).
14. T. W. Ebbesen, H. J. Lezec, H. F. Ghaemi, T. Thio, and P. A. Wolff, "Extraordinary optical transmission through sub-wavelength hole arrays," *Nature* **391**(6668), 667–669 (1998).
15. N. C. Lindquist, P. Nagpal, A. Lesuffleur, D. J. Norris, and S.-H. Oh, "Three-dimensional plasmonic nanofocusing," *Nano Lett.* **10**(4), 1369–1373 (2010).
16. C. Lin, M. T. Berry, R. Anderson, S. Smith, and P. S. May, "Highly luminescent NIR-to-visible upconversion thin films and monoliths requiring no high-temperature treatment," *Chem. Mater.* **21**(14), 3406–3413 (2009).
17. A. Polman, "Applied physics. Plasmonics applied," *Science* **322**(5903), 868–869 (2008).
18. T. Lee, R. P. Trivedi, and I. I. Smalyukh, "Multimodal nonlinear optical polarizing microscopy of long-range molecular order in liquid crystals," *Opt. Lett.* **35**(20), 3447–3449 (2010).
19. Q. C. Sun, H. Mandoor, J. C. Ribot, V. Singh, I. I. Smalyukh, and P. Nagpal, "Plasmon-enhanced energy transfer for improved upconversion of infrared radiation in doped-lanthanide nanocrystals," *Nano Lett.* **14**(1), 101–106 (2014).
20. J. F. Suyver, A. Aebischer, D. Biner, P. Gerner, J. Grimm, S. Heer, K. W. Kramer, C. Reinhard, and H. U. Gudel, "Novel materials doped with trivalent lanthanides and transition metal ions showing near-infrared to visible photon upconversion," *Opt. Mater.* **27**(6), 1111–1130 (2005).
21. B. S. Cao, Y. Y. He, L. Zhang, and B. Dong, "Upconversion properties of Er³⁺-Yb³⁺:NaYF₄ phosphors with a wide range of Yb³⁺ concentration," *J. Lumin.* **135**, 128–132 (2013).
22. M. G. Nikolić, D. J. Jovanović, and M. D. Dramićanin, "Temperature dependence of emission and lifetime in Eu³⁺- and Dy³⁺-doped GdVO₄," *Appl. Opt.* **52**(8), 1716–1724 (2013).
23. H. A. Atwater, "The promise of plasmonics," *Sci. Am.* **296**(4), 56–62 (2007).
24. J. A. Schuller, E. S. Barnard, W. Cai, Y. C. Jun, J. S. White, and M. L. Brongersma, "Plasmonics for extreme light concentration and manipulation," *Nat. Mater.* **9**(3), 193–204 (2010).
25. P. Nagpal, N. C. Lindquist, S.-H. Oh, and D. J. Norris, "Ultrasoft patterned metals for plasmonics and metamaterials," *Science* **325**(5940), 594–597 (2009).
26. N. J. Halas, S. Lal, W.-S. Chang, S. Link, and P. Nordlander, "Plasmons in strongly coupled metallic nanostructures," *Chem. Rev.* **111**(6), 3913–3961 (2011).
27. M. Durach, A. Rusina, V. I. Klimov, and M. I. Stockman, "Nanoplasmonic renormalization and enhancement of Coulomb interactions," *New J. Phys.* **10**(10), 105011 (2008).
28. J. Zhao, Z. Lu, Y. Yin, C. McRae, J. A. Piper, J. M. Dawes, D. Jin, and E. M. Goldys, "Upconversion luminescence with tunable lifetime in NaYF₄:Yb,Er nanocrystals: role of nanocrystal size," *Nanoscale* **5**(3), 944–952 (2013).
29. Y. Li, J. Zhang, X. Zhang, Y. Luo, X. Ren, H. Zhao, X. Wang, L. Sun, and C. Yan, "Near-infrared to visible upconversion in Er³⁺ and Yb³⁺ codoped Lu₂O₃ nanocrystals: enhanced red color upconversion and three-photon process in green color upconversion," *J. Phys. Chem. C* **113**(11), 4413–4418 (2009).

1. Introduction

Upconversion photoluminescence (UPL) has been investigated for potential applications such as biological imaging and solar cell [1–6]. While the infrared photons have insufficient energy to generate photocurrent in a photovoltaic or photodetection device, combining two or more infrared photons to generate a single visible or ultraviolet photon, a process known as upconversion [7], can provide important opportunities for enhancing photovoltaic conversion efficiencies or imaging infrared radiation. Doped-lanthanide nanocrystals provide an alternative as upconverting nanoparticles (UCNP), and a model system to study important photophysical processes like quenching, phonon-assisted and other exciton decay mechanisms (radiative and non-radiative relaxation), weak Purcell effect or electromagnetic field enhancement, energy transfer between dopant ions, and dynamics in multiple photoexcited states (Fig. 1(a)) [4, 7–9]. While several approaches have been utilized to improve the upconversion luminescence enhancement, like surface plasmon polariton, energy migration through core-shell structure, broadband sensitization, and energy clustering [10–13], we carefully analyzed the role of surface plasmon polaritons on these photophysical processes.

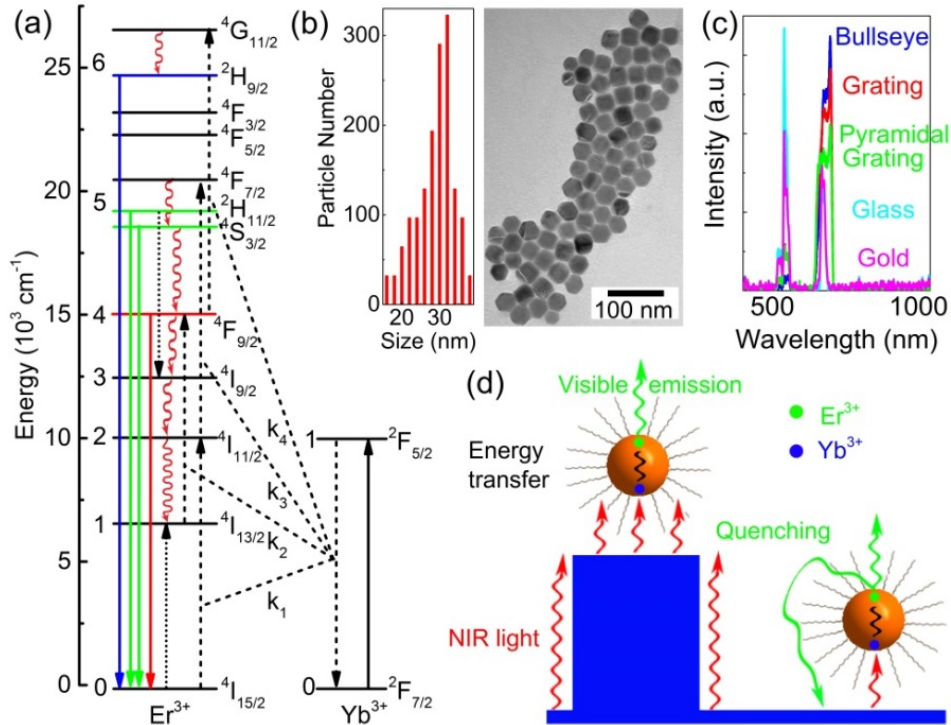


Fig. 1. (a) Energy-level diagram, upconversion excitation, and visible emission schemes for the Yb^{3+} -sensitized Er^{3+} system [7, 9]. Dashed, solid, curly, and dotted arrows indicate upconversion energy transfer, radiative, multiphonon, and cross-relaxation processes, respectively. High efficiency of UPL can be achieved by improving the absorption in Yb^{3+} dopants and enhancing the energy transfer between Er^{3+} and Yb^{3+} (dashed lines). Yb^{3+} mainly absorbs 980 nm photons. (b) Left: the size distribution obtained from several TEM images. Right: a representative transmission electron micrograph (TEM) image of 29 nm $\beta\text{-NaYF}_4:17\%\text{Yb}^{3+}/3\%\text{Er}^{3+}$ nanoparticles. (c) Upconversion emission spectra of 29 nm $\beta\text{-NaYF}_4:17\%\text{Yb}^{3+}/3\%\text{Er}^{3+}$ nanoparticles on linear grating (red curve), bullseye (blue curve), pyramidal grating (green curve), glass (cyan curve), and gold (magenta curve) substrates. (d) Schematic of the energy transfer, upconversion, and quenching processes on the top and bottom of the gold substrate. The doped-lanthanide UCNPs provide a good platform to study all of these photophysical processes.

To evaluate the effect of plasmon-enhancement on the different photophysical processes, we used co-doped $\beta\text{-NaYF}_4:3\%\text{Er},17\%\text{Yb}$ nanocrystals as UCNP. We also fabricated different plasmonic substrates, like linear gratings, bullseye, and pyramid structures on linear gratings, with different plasmon-enhancements and spatially varying electromagnetic field enhancements (Table 1). While the generation of surface plasmons on these ultrasmooth patterned substrates resulted in simultaneous improvement of absorption of infrared radiation (in dominant Ytterbium ions), using weak electromagnetic or Purcell enhancement [11, 14, 15], and enhanced energy transfer rates between minority Erbium dopant and Ytterbium ions to enhance upconversion, they also enhance the quenching and non-radiative relaxation of photogenerated charges to reduce the upconversion efficiency. Therefore, we utilized spectrally-resolved confocal (or depth-resolved) imaging, steady state and time-resolved upconverted photoluminescence measurements, and our theoretical model to decouple these effects.

Table 1. Summary of Electromagnetic (EM) Enhancement, Energy Transfer Enhancement, Nonradiative Decay, and Quenching with Different Plasmon-Enhancements^a

Substrate	EM enhancement	Energy transfer	Nonradiative decay	Quenching
Glass	1	1	1	1
Linear Grating	2	3.2	1.4	2.4
Bullseye	2	3.4	1.8	3.6
Center of Bullseye	2.5	4.3	-	3.9
Pyramidal grating	5	5.1	1.6	9.4

^aWhile Enhancement of electromagnetic field and energy transfer enhances UPL, enhanced non-radiative decay and quenching can decrease upconversion efficiency.

2. Experimental synthesis and setup

The co-doped β -NaYF₄:3%Er,17%Yb nanocrystals were synthesized by a thermal decomposition method [16]. In a typical synthesis, 90 mg Y₂O₃, 33.3 mg Yb₂O₃, and 5.7 mg Er₂O₃ were dissolved in 2 mL CH₃COOH. The lanthanide solution was prepared by dissolving this mixture in 6mL of oleic acid, and heating it to 100 °C under vacuum for 60min. The fluoride-containing solution was synthesized by dissolving 82.0 mg CH₃COONa and 83.5 mg NaF in 2mL of oleic acid and 10 mL of 1-octadecene at 100 °C under a vacuum for 30 min. The fluoride solution was then heated under nitrogen to 320 °C, and the lanthanide solution was injected within 1 min. The homogeneous, single-phase reaction mixture was maintained at 320°C for 30 min under nitrogen, and then allowed to cool to room temperature. The nanoparticles were then precipitated by the addition of 100 mL of acetone, and isolated by centrifugation at 5000 rpm. The samples were re-dispersed and then washed with acetone at least three times. The final products were suspended in toluene for transmission electron microscopy (TEM) characterization and further experiments. Figure 1(b) shows TEM image of 29 nm β -NaYF₄:17%Yb³⁺/3%Er³⁺ nanoparticles and their size distribution. The plasmonic substrates were fabricated using optical lithography and ion etching (for linear gratings and bullseye), or self-limiting anisotropic KOH etching for pyramids, on a silicon template. The patterned silicon template was then coated with ~250 nm of gold film by thermal evaporation, and the ultrasmooth plasmonic substrates were removed with epoxy adhesive [16,17]. The gold patterned arrays were then coated with a uniform layer of UCNP's (Fig. 1(d)), and excited with 980 nm infrared light to measure their steady state upconverted fluorescence (using an Ocean Optics USB4000 spectrometer, Fig. 1(c)).

To analyze the effect of plasmon-enhancement on upconversion photoluminescence, confocal (or depth-resolved) multiphoton fluorescence imaging was performed by excitation with a 980 nm femtosecond pulse from a tunable (680-1080 nm) Ti:Sapphire oscillator (140 fs, 80 MHz, Chameleon Ultra-II, Coherent), and by epi-detection with various interference filters used to separate the fluorescent light from the excitation laser beam [18]. The nonlinear optical process of two-photon absorption by β -NaYF₄:17%Yb³⁺/3%Er³⁺ UCNP (Fig. 2) allows better spatial resolution with spectrally-resolved two-photon excitation fluorescence microscopy imaging, which was obtained for red and green emissions here by using filters. The spatial and multispectral resolution allows mapping of upconverted fluorescence with different plasmon-enhancements along the substrate. Steady-state and time-resolved photoluminescence spectra was also collected to evaluate the occupation of different photophysical states of Erbium dopant, and measure their respective radiative decay rates (Fig. 3).

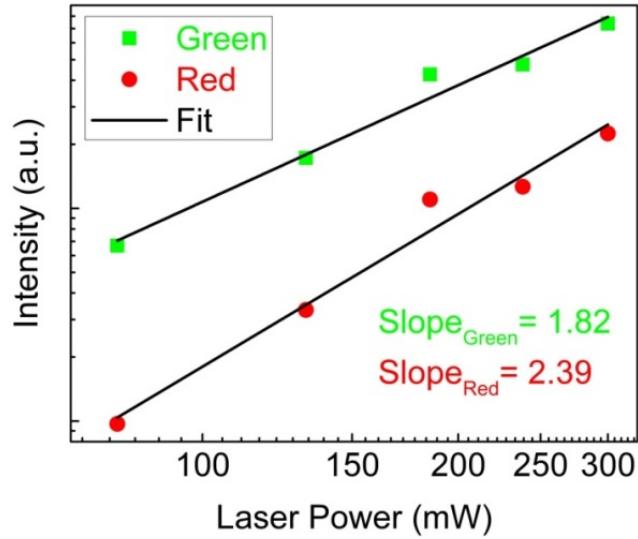


Fig. 2. Pump power dependence of upconversion emission intensities of 29 nm NaYF₄:Yb³⁺/Er³⁺ particles. The slope is ~ 2 which indicates two-photon process.

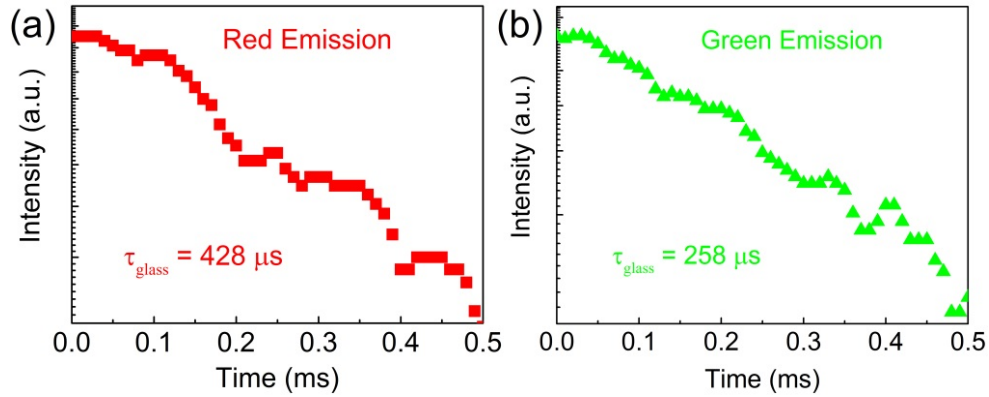


Fig. 3. Time-resolved upconversion photoluminescence (UPL) spectroscopy for (a) red and (b) green emission, respectively. The single-exponential UPL decay indicates small non-radiative relaxation from respective energy levels, and the decay times indicates respective rates of radiative decay.

3. Experimental results and discussions

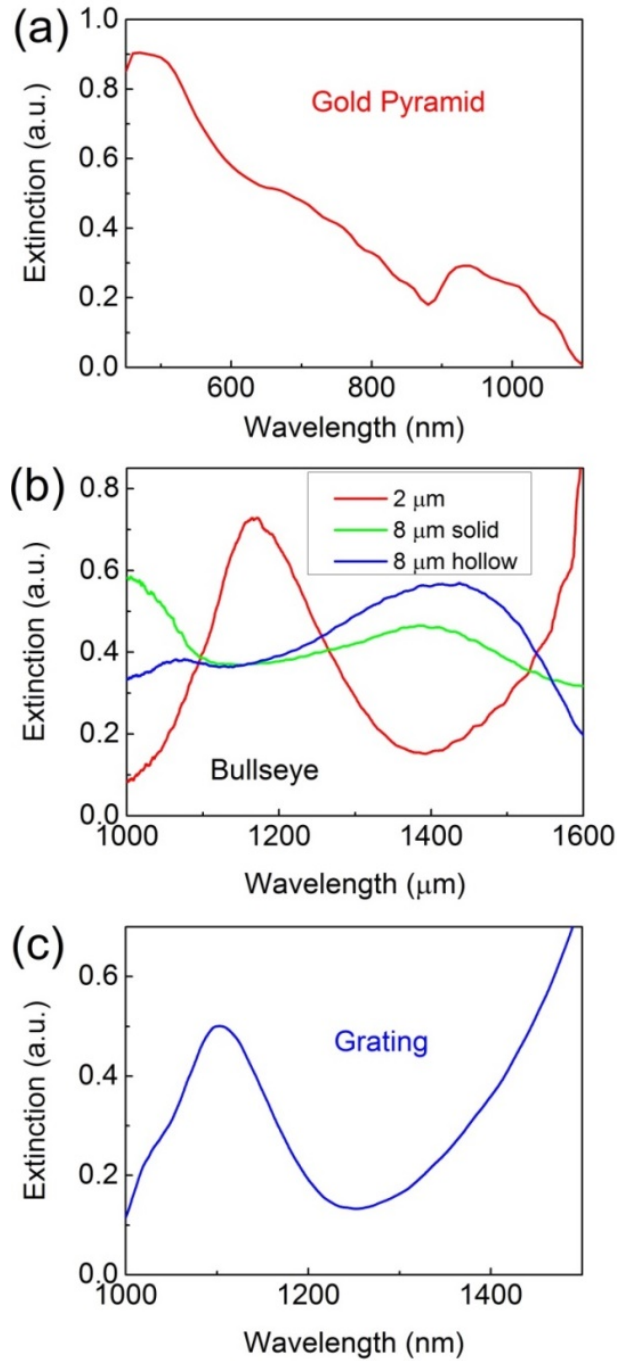


Fig. 4. Near-infrared extinction spectrum for (a) pyramid, (b) bullseye, and (c) linear grating substrates. The plasmon absorption peak shifts to lower wavelength with decreasing periodicity (as shown for bullseye in Fig. 4(b)), indicating shift of respective resonant plasmon energies.

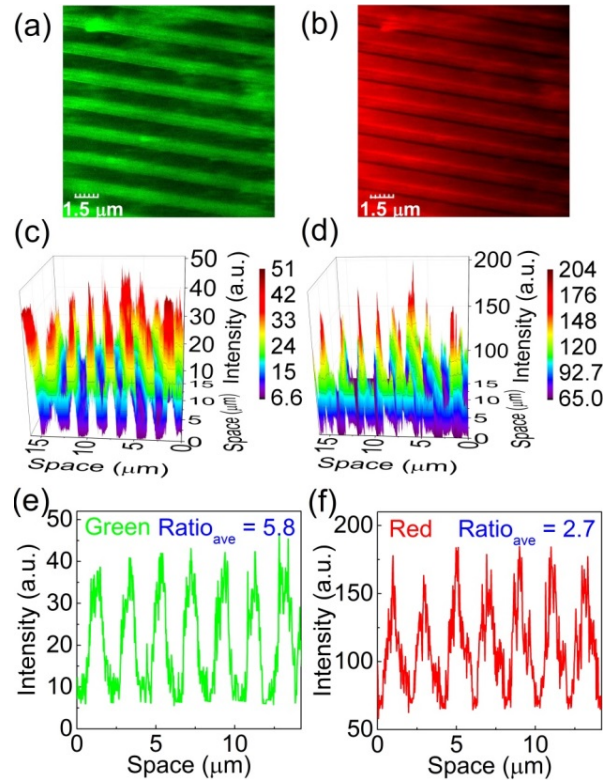


Fig. 5. (a,b) 2D confocal images for the green and red emission of 29 nm β -NaYF₄:Yb³⁺/Er³⁺ particles on the linear grating substrate, respectively. (c,d) 3D confocal scan images of the green and red emission of UCNPs on the linear grating substrate, respectively. (e,f) Spatially resolved line intensity for the green and red upconversion emission on the linear grating substrate, using the 3D image.

The UCNP's (Fig. 1(b)) in films were resonantly excited (Fig. 4) on grating (Figs. 5 and 6), bullseye (Figs. 6 and 7), and pyramidal grating (Figs. 6 and 8) substrates, using 980 nm infrared laser. The periodicity of the pattern was chosen so the surface plasmon resonance (~980 nm) can enhance the infrared absorption and the rate of energy transfer to Erbium, using Coulomb coupling [19]. The green and red upconverted emissions observed at 660nm (red) and 550nm (green) (Fig. 1(c)) corresponded to the transitions $^4F_{9/2} \rightarrow ^4I_{15/2}$ and $^2H_{11/2}$, $^4S_{3/2} \rightarrow ^4I_{15/2}$ in excited Er³⁺ dopant, respectively, and represent the radiative decay observed from these photophysical states respectively. The ratio of UPL intensity from $^2H_{11/2} \rightarrow ^4I_{15/2}$ and $^4S_{3/2} \rightarrow ^4I_{15/2}$ transitions on the different substrates, provides a measure of their respective non-radiative decay rates by emission of multiple phonons. The energy gap between these two thermally coupled states was about 600 cm⁻¹, as estimated from the upconversion emission spectra [20]. Since the UPL ratio of these levels on respective plasmonic substrates depended on the thermalization process [21, 22], this ratio provides a measure of their respective photoexcited carrier temperature and the non-radiative decay rates. According to a Boltzmann-type population distribution, the intensity ratio of green upconversion emissions

can be presented as, $R = \frac{I_H}{I_S} = B \exp\left(\frac{-\Delta E}{k_B T}\right)$, where $\Delta E = 600 \text{ cm}^{-1}$, k_B is Boltzmann constant,

and B is a constant. By assuming that the temperature of the sample on the glass substrate is 300 K, we estimated the respective carrier temperatures of the substrates (using the ratios (R) observed in Fig. 1(c)), and hence the respective enhancement of non-radiative decay rates as a function of plasmon-enhancement, as shown in Table 1.

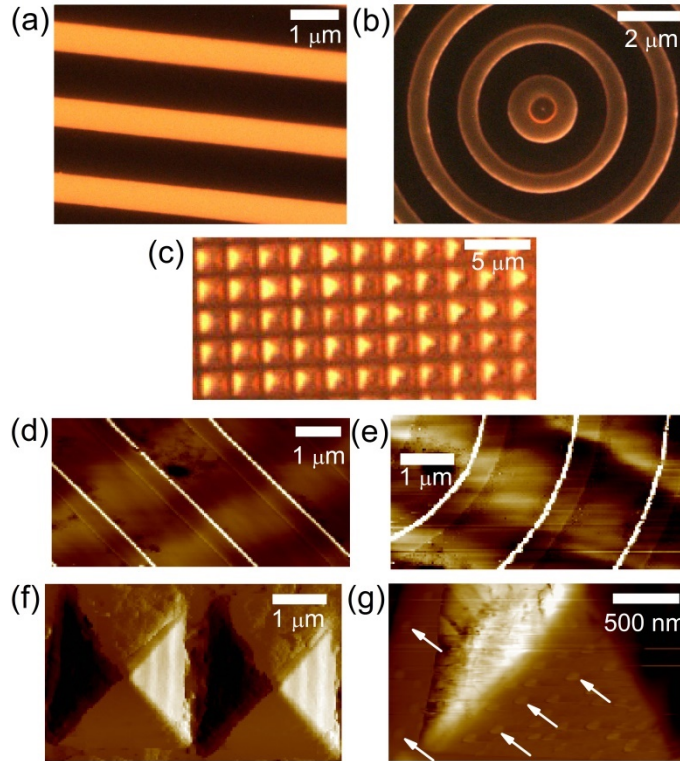


Fig. 6. Optical images of (a) linear grating, (b) bullseye, and (c) pyramid substrates. Atomic force microscopy (AFM) images of (d) linear grating, (e) bullseye, and (f) pyramid substrates. (g) AFM image of the pyramid substrate with 29 nm β -NaYF₄:Yb³⁺/Er³⁺ particles. White arrows point out a few nanoparticles on the pyramid substrate as examples.

Since surface plasmon polaritons (SPP) waves produce large fluctuations of charges (and electric field), resonant with the incident light waves [11, 14, 15, 17, 23–26], they exert a strong Coulombic effect on the near-field electronic and photophysical phenomenon [27]. Using resonant SPP waves on a linear grating substrate, with uniform plasmon-enhancement along the gratings, we analyzed the spatially-resolved multispectral UPL data from UCNPs coated on the substrate (Fig. 5). Using 980 nm incident light, the green (Figs. 5(a) and 5(c)) and red UPL (Figs. 5(b) and 5(d)) from these UCNPs coated on the grating substrate showed uniform enhancement along the grating (Figs. 5(a) and 5(b)). Further analysis of respective upconversion enhancements, for different emitted light frequencies (representing respective radiative emission rates from Erbium states), revealed that average enhancement observed in green emission (~ 5.8 , Fig. 5(e)) was higher than the red emission (~ 2.7 , Fig. 5(f)). Moreover, since the plasmon-enhancement can affect the respective photophysical rates (Table 1) and the resultant UPL enhancement, we designed and fabricated different substrates like bullseye (Fig. 7) and pyramids on linear grating (Fig. 8), resonant with UCNPs absorption (~ 980 nm), to understand the effect of plasmon-enhancement on respective multispectral UPL enhancement (eg, green enhancement in Figs. 7(a), 7(c), 7(e), 8(a), 8(c), and 8(e) and red enhancement in Figs. 7(b), 7(d), 7(f), 8(b), 8(d), and 8(f)).

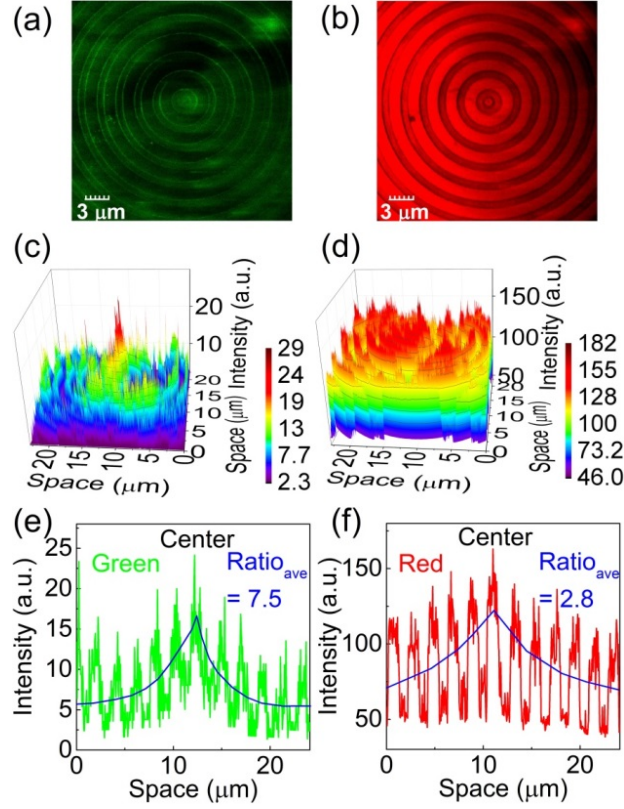


Fig. 7. (a,b) 2D confocal images for the green and red emission of 29 nm β -NaYF₄:Yb³⁺/Er³⁺ particles on the bullseye substrate, respectively. (c,d) 3D confocal scan images of the green and red emission of UCNPs on the bullseye substrate, respectively. (e,f) Spatially resolved line intensity for the green and red upconversion emission on the bullseye substrate, using the 3D image.

To decouple the respective photophysical rates using our spatially resolved multispectral UPL data, we developed a model describing photoexcitation, energy transfer, radiative and non-radiative recombination and occupation of different Er³⁺ energy levels [7, 19, 28]. We also conducted experimental measurements (Figs. 2, 3, and 9) to understand relative importance of the photophysical processes.

$$0 = W_{21}N_{Er,2} - k_2N_{Er,1}N_{Yb,1}, \quad (1)$$

$$0 = k_1N_{Er,0}N_{Yb,1} - k_3N_{Er,2}N_{Yb,1} - W_{21}N_{Er,2}, \quad (2)$$

$$0 = k_2N_{Er,1}N_{Yb,1} - W_4N_{Er,4}, \quad (3)$$

$$0 = k_3N_{Er,2}N_{Yb,1} - W_5N_{Er,5}, \quad (4)$$

$$0 = fI\sigma_{Yb}N_{Yb,0} - k_1N_{Er,0}N_{Yb,1} - k_2N_{Er,1}N_{Yb,1} - k_3N_{Er,2}N_{Yb,1}. \quad (5)$$

Where, k is the energy transfer coefficient, N_i is the electron population of level i of Er³⁺ or Yb³⁺, W_{21} indicates the nonradiative relaxation rate from level 2 to level 1 of Er³⁺, W_4 and W_5 are the radiative decay rates of level 4 and 5 of Er³⁺, σ_{Yb} is the absorption cross section between level 0 and 1 of Yb³⁺, and I is the pump flux and fI is the effective pump flux because the emission of Yb³⁺ is proportional to the absorption. Our analysis revealed several important insights into the photophysics of this coupled system.

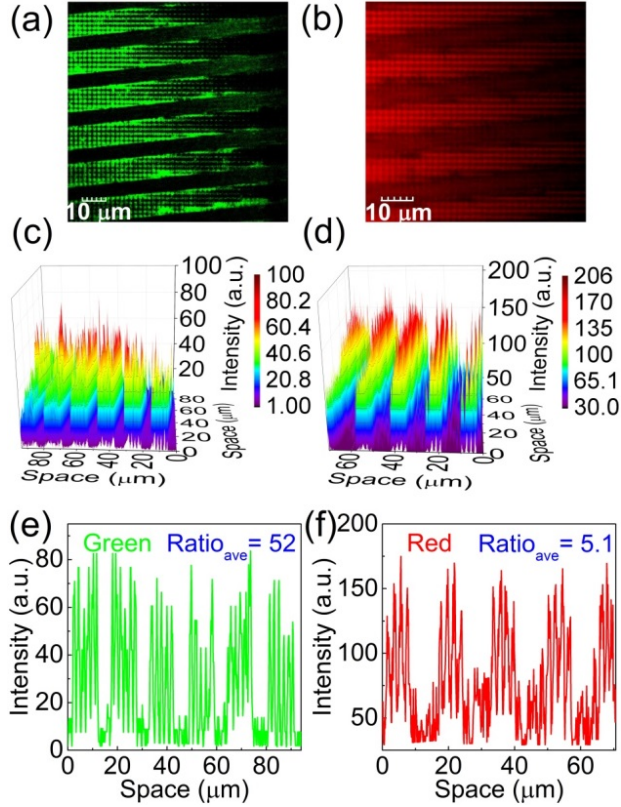


Fig. 8. (a,b) 2D confocal images for the green and red emission of 29 nm β -NaYF₄:Yb³⁺/Er³⁺ particles on the pyramidal grating substrate, respectively. (c,d) 3D confocal scan images of the green and red emission of UCNP on the pyramidal grating substrate, respectively. (e,f) Spatially resolved line intensity for the green and red upconversion emission on the pyramidal grating substrate, using the 3D image.

Using the experimental data, along with estimates of respective carrier temperatures and enhancement of respective non-radiative decay as a function of plasmon-enhancement (Table 1), we observed that green UPL emission was strongly quenched on flat gold (Figs. 5(c), 7(c), and 8(c)), whereas red emission was relatively unaffected (Figs. 5(d), 7(d), and 8(d)). To account for this morphology dependent quenching, we modified Eq. (4) to include quenching:

$$0 = k_3 N_{Er,2} N_{Yb,1} - W_5 N_{Er,5} - k_q N_{Er,5}. \quad (6)$$

Where, k_q is the quenching factor. This wavelength-dependence of quenching is not surprising, since generation of propagating SPP waves can lead to strong quenching close to SPP wavelength (above SPP, additional momentum is required which is not present on ultrasmooth gold [25]). Therefore, while appreciable quenching is not observed for red emission (Fig. 1(c)), the green emission is quenched on flat metal (Figs. 5(c), 7(c), and 8(c)), leading to large apparent UPL enhancements and inverted ratios of green to red emission (Fig. 1(c)). Therefore, we can successfully decouple the effects of electromagnetic enhancement, quenching (k_q), and increased phonon cooling rates due to generation of plasmon waves (Table 1).

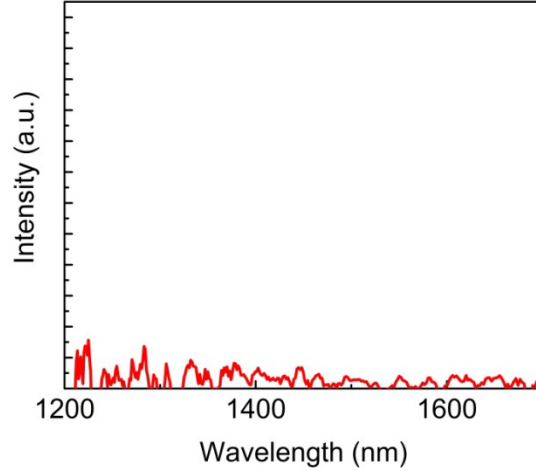


Fig. 9. Near-infrared upconversion emission spectra of 29 nm β -NaYF₄:17%Yb³⁺/3%Er³⁺ nanoparticles on the pyramid substrate.

To understand the effect of generation of plasmon waves on energy transfer rates (from Yb³⁺ to Er³⁺), we analyzed the experimental results for the sample on the glass substrate first.

Using Eqs. (1), (2), and (5), we obtained $N_{Yb,1} = \frac{fI\sigma_{Yb}N_{Yb,0}}{2k_1N_{Er,0}}$. We then assumed that $N_{Yb,0}$ and

$N_{Er,0}$ were approximately equal to the total density of Yb³⁺ and Er³⁺ ions in nanoparticles at a low pumping level considering the fact that long after the pulse has ceased [28]. Therefore,

$N_{Yb,1} = \frac{fI\sigma_{Yb}N_{Yb}}{2k_1N_{Er}}$. Using Eqs. (1), (3), and (4), we obtained $W_4N_{Er,4} = W_{21}N_{Er,2}$ and $W_5N_{Er,5} =$

$k_3N_{Er,2}N_{Yb,1}$, and the green to red ratio was found to be

$R_{G/R} = \frac{W_5N_{Er,5}}{W_4N_{Er,4}} = \frac{k_3}{W_{21}} \frac{fI\sigma_{Yb}N_{Yb}}{2k_1N_{Er}} = 2.18$ for the glass substrate (Fig. 1(c)). This linear pump

power dependence matches with other reported literature [29]. Therefore, the phonon relaxation constant strongly enhanced by the vibrational quanta by the surface hydroxyl

group, $W_{21} = \frac{k_3}{2.18} \frac{fI\sigma_{Yb}N_{Yb}}{2k_1N_{Er}}$, was obtained [29]. Using $W_{21}(T) = W_{21}(0) \left(\frac{1}{\exp\left(\frac{\hbar\omega}{k_B T}\right) - 1} + 1 \right)^p$

[22], where, k_B is the Boltzmann constant, T is temperature, and p is the number of phonons that the ion transfers to the lattice, which depends on the energy difference between the lower and excited states, ΔE , as well as the dominant phonon energy of the lattice $\hbar\omega$ ($p = \frac{\Delta E}{\hbar\omega}$).

Within the temperature range in Table 1, W_{21} is a constant. For the red UPL of the

nanoparticles, we get $N_{Er,2} = \frac{k_1N_{Er}N_{Yb,1}}{W_{21} + k_3N_{Yb,1}}$ using Eq. (2). On the bottom of substrates (Figs.

5, 7, and 8), the emission of level 4 was given as $W_4N_{Er,4} = W_{21}N_{Er,2} = W_{21} \frac{k_1N_{Er}N_{Yb,1}}{k_3N_{Yb,1} + W_{21}}$. On

the top of substrates, FDTD calculation showed electromagnetic enhancements $b = 2$ ($I' = 2I$) at the top of gold grating (Fig. 5), $b = 2.5$ for the bullseye center (Fig. 7), and $b = 5$ ($I' = 5I$) at the apex for patterned gold pyramid (Fig. 8). Because of the strong absorption of 980 nm light

for gold substrates, the resonant energy transfer rate k_1 should be enhanced as $k'_1 = ak_1$, but the non-resonant energy transfer between level 0 and level 5 remains $k'_3 = k_3$ (the energy is far away from the plasmon resonance). The emission from level 4 on the top of substrates was given as $W'_4 N'_{Er,4tip} = W_{21} N'_{Er,2} = W_{21} \frac{k'_1 N'_{Er} N'_{Yb,1}}{k'_3 N'_{Yb,1} + W_{21}}$. Therefore, we obtain the enhancement

(top to bottom ratio) for the red emission as, $R_{red} = \frac{1.459b}{\frac{b}{a} + 0.459}$. Using the red ratio and

electromagnetic enhancement (b), we obtained the energy transfer enhancement (a) of 3.2 for the linear grating, 4.3 at the center of bullseye pattern (due to plasmon nanofocusing), and the highest enhancement of 5.1 for the pyramids on a linear grating (Table 1).

While higher plasmon-enhancement in pyramids leads to very high UPL enhancements, especially for green emission (52 compared to 6.8 and 5.8 for bullseye and linear grating, Figs. 8(e), 7(e), 5(e)), the red UPL emission enhancements are more modest (5.1 compared to 2.8 and 2.7 for bullseye and linear grating, Figs. 8(f), 7(f), and 5(f)). This difference in multispectral UPL enhancement can be explained by different rates of quenching from Erbium energy levels (Table 1). Using the green UPL enhancement from UCNP's on linear grating, bullseye and pyramidal grating substrates, the emission of level 5 was given as,

$W_5 N_{Er,5} = \frac{W_5 k_3 N_{Er,2} N_{Yb,1}}{W_5 + k_q}$, on the bottom of substrate; and $W'_5 N'_{Er,5tip} = k'_3 N'_{Er,2} N'_{Yb,1}$ on the

top of the substrate. Therefore, we got the top to bottom ratio of the green emission as,

$R_{green} = \frac{b(W_5 + k_q) N'_{Er,2}}{aN_{Er,2} W_5}$. Using the green UPL enhancement (Figs. 5(e), 7(e), and 8(e)), we

obtain the quenching enhancement factor (k_q) of 2.4 for the linear grating substrate, 3.9 at the center of bullseye structure, and 9.4 for the pyramids on a linear grating (Table 1).

4. Conclusion

In conclusion, we found that the plasmon-enhancement increases the upconversion fluorescence in lanthanide-doped UCNP's. Our spatially-resolved multi-photon confocal measurements, combined with steady-state UPL and our theoretical model shows that the enhancement occurs due to a combination of weak-Purcell enhancement and increased energy transfer rates. The highest enhancement of energy transfer rates occurs on pyramidal grating substrate (5.1 times, Table 1), due to high plasmon-enhancement and strong Coulomb coupling. While the multispectral enhancements vary between different wavelengths, strong quenching of green emission occurs (shown with different plasmon-enhancements, Table 1) due to propagating SPP waves on flat metal substrate. These results point to the need for careful coupling of plasmon modes with the desired photophysical processes. These findings can benefit the design of biological and renewable energy applications using UPL, and have important implications for modulating the photophysics using generation of surface plasmon polariton waves.

Acknowledgments

Financial support for this work was provided by start-up funds from University of Colorado and NSF Career Award CBET-1351281.